Climate **2015**, *3*, 727-752; doi:10.3390/cli3030727

OPEN ACCESS

climate

ISSN 2225-1154

www.mdpi.com/journal/climate

Article

Linear and Non-Linear Approaches for Statistical Seasonal Rainfall Forecast in the Sirba Watershed Region (SAHEL)

Abdouramane Gado Djibo [1,2,*], Harouna Karambiri [1], Ousmane Seidou [2], Ketvara Sittichok [2], Nathalie Philippon [3], Jean Emmanuel Paturel [4] and Hadiza Moussa Saley [5]

[1] International Institute for Water and Environmental Engineering (2iE), 01 BP 594, Ouagadougou 01, Burkina Faso; E-Mail: harouna.karambiri@2ie-edu.org

[2] Department of Civil Engineering, University of Ottawa, Ottawa, ON K1N 6N5, Canada; E-Mails: Ousmane.Seidou@uottawa.ca (O.S.); ksitt028@uottawa.ca (K.S.)

[3] Centre de Recherches de Climatologie, UMR6282 Biogéosciences CNRS, Université de Bourgogne, Dijon 21000, France; E-Mail: Nathalie.Philippon@u-bourgogne.fr

[4] Institut de Recherche pour le Développement (IRD), Abidjan 08 BP 3800, Côte d'Ivoire; E-Mail: manupaturel@gmail.com

[5] Centre Africain d'Études Supérieures en Gestion (CESAG), Dakar BP 3802, Sénégal; E-Mail: hmsaley@gmail.com

***** Author to whom correspondence should be addressed; E-Mail: abdouramanegado@gmail.com; Tel.: +00226-7195-2188.

Received: 19 June 2015 / Accepted: 1 September 2015 / Published: 14 September 2015

Abstract: Since the 90s, several studies were conducted to evaluate the predictability of the Sahelian rainy season and propose seasonal rainfall forecasts to help stakeholders to take the adequate decisions to adapt with the predicted situation. Unfortunately, two decades later, the forecasting skills remains low and forecasts have a limited value for decision making while the population is still suffering from rainfall interannual variability: this shows the limit of commonly used predictors and forecast approaches for this region. Thus, this paper developed and tested new predictors and new approaches to predict the upcoming seasonal rainfall amount over the Sirba watershed. Predictors selected through a linear correlation analysis were further processed using combined linear methods to identify those having high predictive power. Seasonal rainfall was forecasted using a set of linear and non-linear models. An average lag time up to eight months was obtained for all models. It is found that the combined linear methods performed better than non-linear, possibly because non-linear models require larger and better datasets for calibration. The R^2, Nash and Hit rate score are

respectively 0.53, 0.52, and 68% for the combined linear approach; and 0.46, 0.45, 61% for non-linear principal component analysis.

Keywords: rainfall forecasting; neural network; non-linear principal component analysis; Sirba basin; West African monsoon; air temperature

1. Introduction

The summer rainfall of semi-arid regions of the world is known for its unreliability, which has a large impact on the continental hydrological cycle, water resources and food security. The Sahel, extending across Africa from the Atlantic Ocean to 30 °E and from 12 to 17 °N is the largest area of these regions, recording between 200 and 800 mm/year from north to south, ~80% of the rain being recorded in July–September the cool rainy season. Temperature in this region ranges from approximately 18 to 36 °C. The recurrent droughts and subsequent famines that struck the Sahel in the 1970s (1972–1974), and the 1980s (1983–1985) and make it unique at the global scale led the scientific community to investigate possible mechanisms responsible for these dramatic events and to develop forecasting models to help coping with such phenomena. This area experienced severe droughts almost every two to three years. The devastate drought in 2012 affected more than 18 million people in nine countries with food insecurity, high grain prices and environmental degradation. This 2012 crisis came after the severe drought in 2010 [1–18].

The Sahelian rainfall pattern is season dependent and is directly related to the West African Monsoon (WAM).

Although, the WAM's dynamic is better understood nowadays, the main challenge with regards to its variability and predictability comes from its varying teleconnections. A teleconnection is the linkage of climate variables between two different areas, which may be close or far to each other [19,20]. Teleconnections between Sahelian rainfall and the oceanic basins have changed quickly much since the 60's: the tropical Atlantic had the strongest influence during the years 60–70, then the equatorial Pacific (El Nino/Southern Oscillation) during the 80–90's, and the Mediterranean now [21–25]. Thus, the absence of well-established predictors that can be used to predict seasonal rainfall as well as streamflow in the Sahel partly explains why forecasts at all scales in the Sahel are tricky. Many studies attempted to forecast Sahelian seasonal rainfall and streamflow for the purpose to overcome the droughts impacts [4,7,26–33]. Unfortunately, most of these works focused on only sea surface temperatures (SST) over years [24,34–36]. Nevertheless, few studies attempted to use the atmospheric dynamics for carrying out seasonal forecasts. This prediction relies on the explicit simulation of major atmospheric processes [37–44]. Garric *et al.* [42] used the ARPEGE atmospheric model forced by SST anomalies and multivariate linear regression using SST and rainfall predictors observed before the monsoon season. They showed that the ARPEGE model did not give better seasonal rainfall predictions than simple regression systems.

Thus, the objective of this paper is to develop a method that would identify new skillful predictors for seasonal rainfall in the Sahel, and to compare a set of linear models to non-linear ones for forecasting JAS (July to September) rainfall amounts. This would provide the community with actionable seasonal

information that would constitutes a major tool for farmers, decision makers and water resources managers in this region.

For such purpose, a pool of predictors is built by analyzing the physical influence on the WAM. Each predictor is tested as an input to a linear rainfall forecasting model as in [4]. At the end of the process, an optimal lag time and an optimal season are obtained to extract the predictor. Retained predictors are afterward also tested in new developed non-linear models. Finally, the forecast skills of the two groups of models are discussed.

2. Review of the Main Drivers of the Sahelian Rainfall Variability

In West Africa, the rainfall pattern is firmly related to the seasonal movement of the inter-tropical convergence zone (ITCZ) and consequently to the development of the WAM circulation [45].

The SST constitutes a key factor in the variability of the WAM and therefore the Sahelian precipitations as shown in several studies [12,34,37,46–48]. The tropical Atlantic Ocean is considered as the principal source of moisture for West Africa. Its impact on the WAM system was shown since 1970s when the Sahelian rainfall deficit was associated to colder SST in the north tropical Atlantic and warmer SST in the south and at the equator which promotes a southernmost ITCZ than the normal. These results were confirmed, and then extended to longer time scales by many studies [13,49–52]. However, Janicot *et al.* [53] noticed that the relationship between Sahelian rainfall and Atlantic SSTs considerably decreased to a point to be statistically not significant during the dry period (*i.e.*, post 1970). This teleconnection changed from Atlantic SST to the SST over eastern and center Equatorial Pacific, in agreement with the work of [54].

A rainy season with below average rainfall in West Africa is usually associated to a warm period of El Niño-Southern Oscillation (ENSO). Janicot *et al.* [55] explained this link by a strengthening of the Walker circulation and a weakening of both the monsoon and the southern cell of the Hadley circulation. This situation leads to an increase in trade winds over the northern tropical Atlantic and a reduction in the water vapor in West Africa. Recently, a teleconnection with the Mediterranean Sea has been highlighted [56–58]. It seems to impact the WAM system in addition to the Atlantic and Pacific [58]. Rowell [56] found that the influence of temperature anomalies in the Mediterranean on the Sahel (for 1947–1996) is of a similar magnitude with that in the Pacific. From numerical simulations, he showed that a warm Mediterranean sea promotes excess rainfall in the Sahel. Additionally, Gaetani *et al.* [57] pointed out that a positive precipitation response to warmer than average conditions in the Mediterranean Sea is found in the Sudano-Sahelian belt in August to September.

Several recent papers analyzed the interactions of the different oceanic basins and the resulting impact on the Sahelian rainfall variability. Shaman and Tziperman [59] found that the interannual rainfall variability over the Mediterranean region is related to ENSO variability in the eastern Pacific *via* an eastward-propagating atmospheric stationary barotropic Rossby-wave train. Moreover, Lopez-Parages *et al.* [60] explained how the teleconnection with the ENSO appears modulated by multidecadal oscillations of the SST over the Atlantic and Pacific basins.

With regards to the role of the land surface on the Sahelian rainfall variability, Webster *et al.* [61] indicated that the use of the moist static energy (MSE) (its three components: sensitive, latent and potential) could improve the rainfall forecasts in the Sahel. They argued that the variation in temperature between the ocean and the continent is responsible for the monsoon circulation; and this circulation is even better

explained when the moisture gradient is considered. Eltahir [62], Philippon and Fontaine [63], Hall and Peyrillé [64] highlighted the role of these gradients on the dynamics of WAM and the Sahelian rainfall variability. Zheng and Eltahir [65] found that a change in vegetation (e.g., deforestation) on the Guinean coast has a direct substantial impact on atmospheric dynamics associated with the monsoon circulation through MSE gradients. Thus, some authors such as Wang and Eltahir [66] suggested the inclusion of vegetation dynamics in the modeling exercises as it constitutes an important process for simulating Sahelian rainfall variability. In addition, while testing the impact of vegetation in rainfall variability simulation, Zeng *et al.* [67] found that the decadal variability is best reproduced when interactive vegetation is added to the model. The role of soil moisture on West African rainfall event is also addressed in some studies [62,68]. These authors emphasized that a positive anomaly of soil moisture would strengthen the monsoon circulation through a modification of MSE gradients. Douville *et al.* [69], Douville [70], and Douville [71] found that any reduction in soil moisture in ARPEGE is associated with low intensities of precipitations. Thus, based on these results they concluded that soil moisture contributes to the interannual variability of rainfall in the Sahel.

It therefore appears that the climate in West Africa (predominantly in the Sahel) is determined by interactions between global processes (e.g., sea surface temperatures) and regional processes (e.g., physiographic characteristics). The use of parameters related to these processes in seasonal rainfall forecasting models would generate more skillful forecasts for the Sahel.

3. Materials and Methods

3.1. Study Area

The study area considered in this work is the Sirba watershed. This watershed, shared by Burkina Faso and Niger, is situated between latitudes 12°55'54"S–14°23'30"N and longitudes 1°27'W–1°23'42"E with an area of 38,750 km^2 (Figure 1) [72]. This choice is motivated by the fact that the Sirba basin is central in the Sahel region, and there are many climate stations inside and around the basin that have been collecting climate data daily for more than 40 years. Another reason is that, locally, the Sirba tributary plays an important role in the hydrological regime of the Niger river at Niamey, as it participates in its Sudanian flood in September. The Sirba extends over three sub-climate zones based on the amount of rainfall decreasing from south to north: a southern Sudanian zone with mean annual rainfall between 700 and 800 mm, a northern Sudanian zone with mean annual rainfall ranging from 550 to 650 mm and a Sahelian zone with mean annual rainfall of 300 to 500 mm [73]. The largest quantities of rainfall are observed during the months of July to September (JAS), regardless of the climate zone. The climate is generally characterized by the presence of two seasons: a dry season (October to April) due to the Harmattan (dry wind) and a rainy season (May to September) influenced by the WAM (wet wind). The hydrographic network is relatively dense and consists of three main tributaries (Sirba, Faga and Yeli) as well as some water reservoirs from dams [71]. Based on the description of the rainfall pattern, the hydrological regime in the Sirba watershed is of Sahelian type, as it is characterized by non-sustainable flows with an exoreic operation pattern. At the upper bed of the Sirba, there is a series of depressions with intermittent flow. However some sections of the Sirba reaches have water constantly during the wettest years. Its vegetation formation is thorny, lightly-wooded savannah.

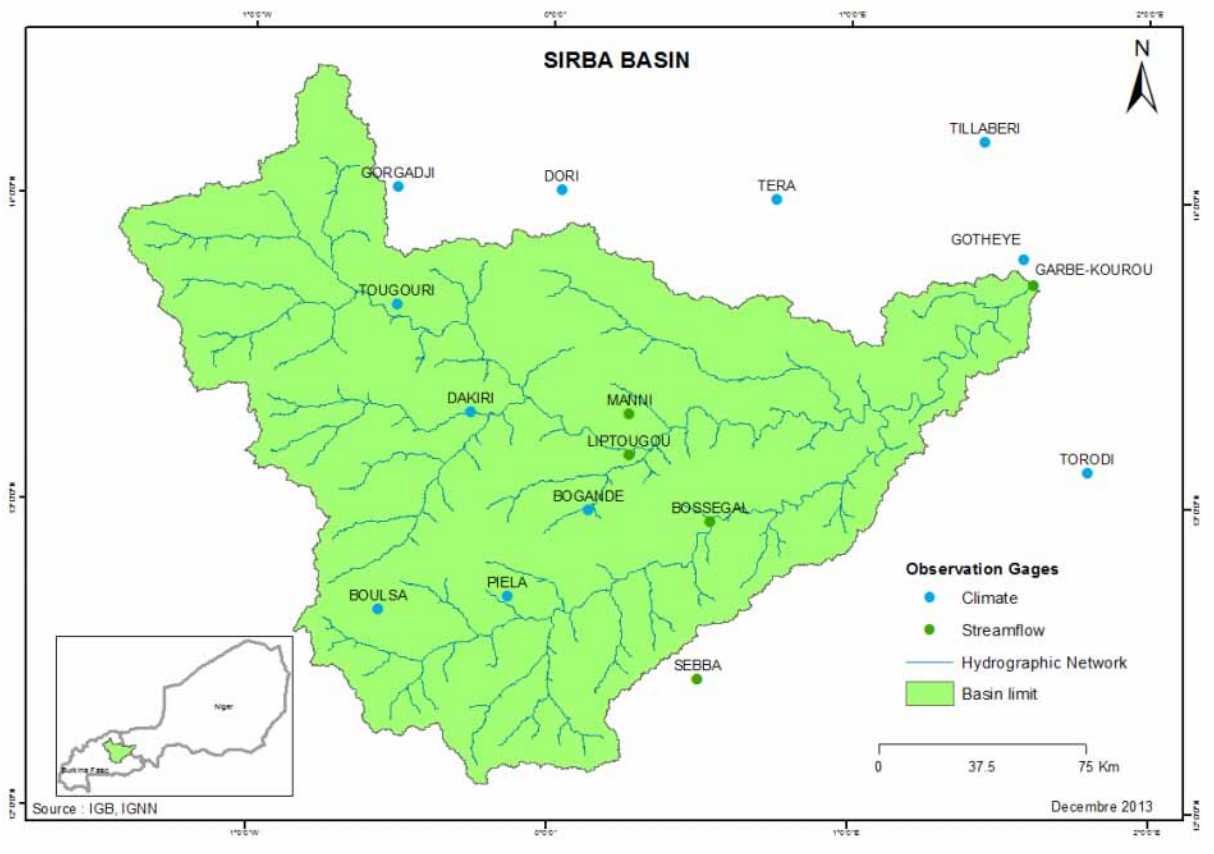

Figure 1. Sirba watershed and observation stations.

3.2. Climate and Atmospheric Data

Climate data used in this study include rainfall and atmospheric data. *In situ* daily rainfall data span the period 1960–2008, and are obtained from national meteorological offices of Burkina Faso and Niger. Five of these stations are located within the watershed while the remaining six stations are located at most 25 km from the watershed boundary (Figure 1). The Thiessen polygon method is a standard method widely used to calculate average areal precipitation [74]. It was implemented to estimate average rainfall over the watershed from the 11 rainfall time series (Table 1). Though there is a lack of good climate data throughout African Sahel, only a few gaps were found in these records, and they do not alter the quality. The *in situ* rainfall time series have less than 10% missing data as this ratio varies from 0 to 7% for all 11 stations over the period. Moreover, monthly precipitation time series of Climatic Research Unit (CRU TS 3.21 0.5 °global) with a spatial resolution of 0.5 ° × 0.5 °and defined on latitudes 10 °N–15 °N, longitudes 2 °W–2 °E are used. They are sourced from the British Atmospheric Data Centre (BADC, http://www.cru.uea.ac.uk/cru/data/hrg/) and span the period 1901–2012 [75].

The atmospheric data considered are Sea Level Pressure (SLP), Sea Surface Temperature (SST), Relative Humidity (RHUM), Air Temperature (AirTemp), Meridional Wind (VWND), and Zonal Wind (UWND). These variables are monthly NCEP-DOE Reanalysis data sourced from the National Oceanic and Atmospheric Administration (NOAA: http://www.esrl.noaa.gov) except the SST data series (NOAA NCDC ERSST version3b sst) obtained from the IRI data library (International Research Institute for Climate and Society: http://iridl.ldeo.columbia.edu) [76]. These data span from January 1979 to August

2013, except for SST data which cover the period January 1960 to December 2013. The relationship of these predictors with the WAM is briefly described in the following paragraphs.

Table 1. Specifics of rainfall stations.

Station number (code)	Station name	Longitude (degrees: °)	Latitude (degrees: °)	Country
320006	Torodi	1.80	13.12	Niger
320002	Tera	0.82	14.03	Niger
320004	Tillaberi	1.45	14.20	Niger
320005	Gotheye	1.58	13.82	Niger
200082	Boulsa	−0.57	12.65	Burkina Faso
200026	Dori	0.03	14.03	Burkina Faso
200085	Bogande	0.13	12.98	Burkina Faso
200048	Dakiri	−0.27	13.30	Burkina Faso
200024	Gorgadji	−0.52	14.03	Burkina Faso
200086	Piela	−0.13	12.70	Burkina Faso
200047	Tougouri	−0.52	13.65	Burkina Faso

(a) Zonal Wind and Meridional Wind

Gallée *et al.* [77] have highlighted the importance of the meridian gradient of MSE on the movement of the ITCZ northward. According to their studies, MSE led the WAM and creates an environment favorable for deep convection over the Sahel. Thus, the spread of WAM to north is associated with strong gradient of MSE in the lower layers, the convergence result in the triggering of convection over the Sahel. These authors emphasized the relationship between the WAM, precipitation, the MSE, the meridian wind and sensible and latent heat in the Sahel. The strong north-south gradient (weak) of the meridian wind seems to be the result of a strong south-north gradient (weak) of MSE. The first maximum MSE gradient develops, followed by the maximum meridian wind. Then the MSE meridian gradient leads meridian wind speed and precipitation to a secondary maximum. In general, changes in precipitation appear to be a consequence of MSE with a major role of the meridian wind.

The zonal and Meridian winds play a very important role in the flow in the middle and upper troposphere. Indeed, in the middle and upper troposphere, the zonal wind profile is dominated by three jets: AEJ (African East Jet), TEJ (Tropical East Jet) and WSJ (West South Jet). AEJ is at the level of 600 hPa and TEJ at 200 hPa. These two jets, which are located above the Sahel and Guinea, are important for the atmospheric dynamics in West Africa. The variation of these winds regulates the position of the AEJ, which, in turn, explains why during wet years (dry) for the Sahel [68,78]. Grist and Nicholson [79] showed evidence of AEJ above the Sahel (10 °N to 15 °N). JET looks very bound to the African monsoon. Indeed, through the Walker circulation, the intensity of the jet effect of the monsoon which forms the lower part of the cell [80]. Sultan [81] shows that the jet's installation date is a good indicator of the development of the monsoon. Finally, Nicholson and Grist [82] suggested that the jet is a response to precipitation but is not a cause of the variability of rainfall.

(b) Air Temperature

The impact of Air temperature on the WAM occurs through a link with atmospheric dynamics over West Africa. According to Fontaine *et al.* [83], the air temperature at two meters presents its maximum before the wet period (during the month of May) because of the maximum exposure at the top of the atmosphere and is followed by a maximum equivalent potential temperature (Θe) in August because of the maximum of the zenith angle of the sun. Θe in the lower troposphere is equivalent to MSE whose transport is due to the circulation of large-scale (the Hadley). But Flaounas *et al.* [84] and Guiavarch *et al.* [85] like other studies have clearly shown the relationship between this surface energy and WAM. Thus, it appears that the relationship between air temperature and the WAM is not a direct link but rather a role on the dynamics of WAM in terms of anomalies reflections in atmospheric circulation like Hadley types.

(c) SST

Several studies have analyzed the relationship between WAM and SSTs. Co ëtlogon *et al.* [86] studied the link between WAM and the contrast between SST and the temperature at the coast of Guinea. According to their results, from spring to summer, a band of cold water settles between Ecuador and the coast of Guinea and enhances the temperature gradient at the surface meridian. This causes the acceleration of the WAM which then moves further north. The appearance of this band of cold water is attributed to the process of recovery in deep and cold ocean masses "upwelling", mostly due to surface winds. Thus, the acceleration of WAM resulted from a positive feedback system since the acceleration intensifies upwelling increasing itself from WAM that spreads further north. Moreover, Peyrill é and Lafore [87] developed a two-dimensional idealized model to reproduce the monsoon system in West Africa. Their study reveals the importance of SST in the Mediterranean. The lack of moisture transport or transport by zonal eddies above the African continent requires forcing external moisture advection in the Mediterranean to get realistic monsoon in West Africa. Thus, they show that warm SST in the Mediterranean entails strengthening moisture advection in the lower layers. SST of West Mediterranean seems to have a stronger impact on the variability of precipitation in the Gulf of Guinea (Sahel) [88]. Several studies suggested some links between the variability of SST during the season of coastal rain and precipitation, especially through the installation of the equatorial upwelling. Gu and Adler [89] describe, using satellite observations and reanalysis, the seasonal evolution of the tropical Atlantic. They show that, in the Gulf of Guinea, convection is modulated by seasonal forcing of the ocean and the SST gradient meridian. In addition, it was shown that the Pacific Ocean [34], the Atlantic Ocean [90], the Mediterranean [88] as well as the phenomenon El Ni ño-Southern Oscillation [10] generate atmospheric disturbances and, in this way, affect the African monsoon.

(d) SLP

A climatological analysis by Baldi *et al.* [91] suggests that the West Africa monsoon influence the central-western [92,93]. Using NCEP/NCAR global reanalysis [91] analyzed in detail the events characterizing summer 2002 over Mediterranean, Europe and North Atlantic, in particular the anomalous SST and Sea Level Pressure (SLP) fields relatively to the mean climate patterns Mediterranean summer, and specifically the SLP (weakly), the temperature and the rainfall. They also found that the overall

pattern of the WAM changed in July, when a lower pressure developed from Iceland to central Mediterranean along a northwest to south-east axis, with anomalously high pressures in the south-west and north-east. Moreover, the summer average SLP field was similar to the pattern observed in July. The surface air temperature field over Mediterranean closely follows the sea level pressure patterns in summer (e.g., Maheras and Kutiel, [94]). They also run sensitivity analysis which shows how the SST anomalies can produce quantitatively significant anomalies in the sea level pressure patterns over North Sahel (positive).

(e) RHUM

The interaction between the flows of heat from the surface of ground water and in the atmosphere has been studied by Lafore [95] and Fontaine *et al.* [88] over the period 1979–2001. Four phases of the ITCZ (inter tropical convergence zone) were identified: early March, mid-April, May and late June (establishment of WAM). These phases appear to be sensitive to the relative humidity of last year. The interaction between these phases is as follows: positive anomalies in this humidity entail an increase in the humidity of the atmosphere, and the convergence of humidity flux- and a decrease in surface albedo. Therefore, the net solar radiation is strengthened on the surface but the air temperature in the lower layers decreases. Net radiation on the surface increases as well as the flow of heat to the atmosphere. This process results in the strengthening of MSE in the lower layers and the strengthening of the circulation of WAM. On the other hand, Fontaine *et al.* [83] showed that in the three regions in West Africa (Guinea, 6 °N–10 °N, Sudan 10 °N–15 °N, the Sahel 15 °N–20 °N), the convergence integrated moisture flux in the entire atmospheric column is significantly correlated with the precipitation at different scales. It is interesting that in the Sahel, unlike the rest of West Africa, the relationship between precipitation and soil evaporation (consequently the RUM) in the Sahel is almost linear. Moreover, Broman *et al.* [96] performed A *K*-means cluster analysis to identify spatially coherent regions of relative humidity variability during the two periods over West African Sahel. They found that correlating the cluster indices with large-scale circulation and SSTs indicates that the land-ocean temperature gradient and the corresponding circulation, tropical Atlantic sea surface temperatures (SSTs), and to a somewhat lesser extent tropical Pacific SSTs all play a role in modulating the timing of the monsoon season relative humidity onset and retreat.

Thus, it is clear that the RUM is a link because it is connected to the mainland that can exert forcing on the atmospheric dynamics through which it is a reflection of abnormalities in the circulation of WAM.

From the above explanation, it is clear that despite that the atmosphere has no inertia the predictors (SLP, AirTemp, and RUM) are connected either to the ocean or continent that can have a forcing on atmospheric dynamics and they are the reflections of anomalies in the atmospheric circulation types Hadley or Walker. Other predictors are related to the Pacific or the Mediterranean to the tropical Atlantic. Table 2 summarizes the atmospheric data and their geographical locations.

3.3. Selection of Predictors and Optimal Lag Time

Monthly CRU precipitation time series cover an area larger than the extent of the Sirba basin. They were initially used as predictand for selecting a pool of potential predictors having a known relationship with the WAM, and to avoid those with no effect on the monsoon dynamics.

Table 2. Description of atmospheric data.

Parameter	Units	Level	Reference Data	Spatial coverage	Regions of the Predictors	Temporal Coverage
Sea level pressures (SLP)	Pa/s	1000 hPa	NCEP 2	2.5 ° × 2.5 °grid 15N–45S, 60W–10E	Atlantic ocean	1979/01/01 to 2013/08/31
Air temperature (AirTemp)	℉K	1000 hPa	NCEP 2	2.5 ° × 2.5 °grid 20N–15S, 120E–70W	Pacific ocean	1979/01/01 to 2013/08/31
Meridional wind (VWND)	m/s	1000 hPa	NCEP 2	2.5 ° × 2.5 °grid 90N–90S, 0–180W	Sahel (Easterly jet)	1979/01/01 to 2013/08/31
Zonal wind (UWND)	m/s	1000 hPa	NCEP 2	2.5 ° × 2.5 °grid 30N–25S 10W–10E	Sahel (Easterly jet)	1979/01/01 to 2013/08/31
Relative humidity (RHUM)	%	1000 hPa	NCEP 2	2.5 ° × 2.5 °grid 40N–30N, 20E–35E	Mediterranean basin	1979/01/01 to 2013/08/31
Sea surface temperature (SST)	℃	Surface	NOAA NCDC ERSST version3b	2 ° × 2 °grid 39N–15S, 60W–15E	Atlantic ocean	1854/01/01 to 2013/08/31
Climatic research unit rainfall (CRU)	mm	Surface	CRU	0.5 ° × 0.5 °grid 2 ℃W–2 ℃E, 10 ℃N–15 ℃N		January 1901 to December 2012

These monthly precipitations time series were averaged over the season July–September (JAS), which is the core of the rainy season in the Sahel. As a preliminary test, different time periods 1960–2010, 1970–2010, 1980–2010, 1990–2010, 2000–2010 are considered to check the most favorable periods in terms of signals within the pool of potential predictors. The reason for testing these sub-periods resulted from the previously mentioned studies (Section 2) which showed that the teleconnections of the Sahelian rainfall have evolved since the 60's. Based on these defined periods, 13 groups (with 89 sub-components) of predictors were considered for the preliminary test to check the presence of significant correlations ($R > 0.5$) between each predictor and CRU rainfall.

After this first selection which relies on the CRU precipitations dataset as predictand, predictors were selected using the *in situ* rainfall (from rain gauge stations) as predictand. This selection is done using the method developed in [4]. This method was employed to link the observed rainfall and each predictor through some statistical techniques. The candidate predictor was aggregated over all possible time windows (where a time window's length in months is an integer) during the 18 months prior to the rainy season onset and each of the obtained time series was used as an explanatory variable in a linear model having the seasonal rainfall on the Sirba watershed as explained variable.

The choice of the period over which the predictor is averaged will impact the performance of the forecast. Since the best period is not known *a priori*, predictor data sets were aggregated over various periods with different lengths and different start dates. The periods were restricted to start at the

beginning of a calendar month and finish at the end of a calendar month. The beginning of a period has to be later or equal to January 1st of the previous year (year Y-1, where Y is the year containing the rainy season for which the forecast is issued).

The end of the period must be prior or equal to June 30th of year Y. Figure 2 shows how time windows were systematically generated. The upper bar indicates all months starting from January of the previous year (year Y-1) to June of the year the forecast is issued (year Y). In the first run, for example, only the predictor of January (Y-1) was selected to use as a predictor. Predictor averaged over January-February (Y-1) was used as a predictor in the second run. This process was iterated at one-month increments until June (Y) was reached as the end of the period. The process was repeated until the beginning and the end of the periods were June (Y).

For each time window, a linear model linking the predictor averaged over that time window and seasonal rainfall on the Sirba was built as follows:

(a) For each year *Y* that the predictor was available,

- (i) The predictor of year *Y-1* was removed from the predictor grid;
- (ii) The rainfall of year *Y* was removed from the rainfall data set;
- (iii) A coefficient of correlation (R) is used to screen the remaining predictor data: a correlation analysis between the predictor at each grid point and the rainfall was computed and its level of significance (P-value <0.05) was assessed. Once the correlation was not significant, the grid point was discarded. The remaining grid points were then ordered decreasingly;
- (iv) Afterward, a principal component analysis (PCA) was applied on the retained predictor gridded data from the previous step to reduce the number of predictors;
- (v) Since PCA gave rise to more sets of new predictor data, a stepwise regression (5% confidence interval) was used to keep only grid points with high predictive power;
- (vi) A linear regression was fitted between the predictors and precipitation time series;
- (vii) The fitted linear regression was used to simulate the rainfall of year *Y*. If predictor and rainfall were in the same year (Year *Y*), only predictor and rainfall time series for that year were removed in the first step.

(b) Then, the coefficient of determination (R^2), Nash-Sutcliffe coefficient (Nash), and Hit-Rate scores (HIT) were computed to estimate the model's performance.

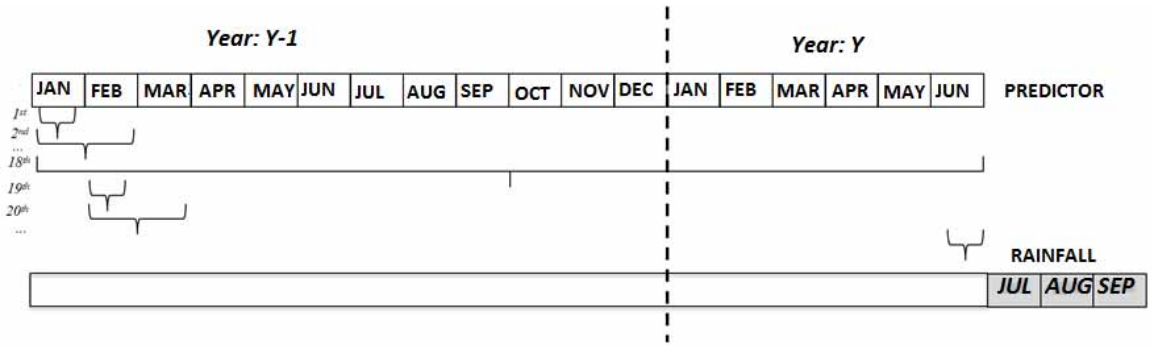

Figure 2. Predictor averaging periods (Adapted from Sittichok *et al.* [4]).

In summary, all predictors were selected according to their physical link with the WAM based on the hypothesis that only predictors having dynamical link with the WAM seem to give good forecast skills. Each of these predictors was screened through simple correlation test to find its link with the CRU rainfall data defined over a region covering more than the Sirba watershed. The main criteria used to find either the predictor should be retained or rejected is the correlation coefficient (R) that has to be greater or equal to 0.5 (*i.e.*, p-value < 0.05). The CRU rainfall was used at this stage for the purpose to have a good assessment of all possible predictors having impact on the WAM. The retained predictors were further screened based on *in situ* rainfall using the approach explained previously and summarized in Figure 2. All these steps were summarized in the new flowchart of Figure 3. It should be noted that the figures provided were based on leave-one out cross validation (LOOV) which was also used is selecting the predictor. The LOOV was used due to the small length of data used.

The first three (3) best predictors in terms of high Nash values were used to test the performance of the two sets of methods (linear approach and non-linear approach).

3.4. Linear Approach

Several linear methods are applied successively for selecting the predictors and developing the seasonal rainfall forecast models. They include: correlation analysis, principal component analysis (PCA), stepwise regression, linear regression, and cross validation.

They were used to perform three successive tasks: predictor selection; predictor dimension reduction and linear regression. The first application discarded meaningless predictors from the original data set using the coefficient of correlation as criteria of selection. At this stage, the correlation coefficient between the predictor at each grid point and the rainfall on the Sirba watershed was calculated and its level of significance (p-value < 0.05) was tested. When the correlation was not significant, the grid point was discarded. The remaining grid points were then decreasingly ordered according to the correlation p-value. Only the best grid points were included in the analysis. Afterward, PCA was applied on the retained predictors to reduce their number. A forward stepwise regression method (5% confidence interval threshold) was then applied to keep predictors having only a significant predictive power.

It should be noted that a leave-one-out cross validation was used in the model application to avoid the bias which might occur during the development of empirical equations using statistical models.

3.5. Non-Linear Approach

Two non-linear methods were tested for each of the three best predictors selected based on the correlation analysis. The description of these methods and how they are applied is detailed in the next paragraphs. The R^2, Nash, and HIT were calculated to estimate the model's performance.

3.5.1. Non-Linear Principal Component Analysis

The non-linear principal component analysis (NLPCA) algorithm developed by [97] is generally considered as a non-linear generalization of standard linear PCA and was successfully applied in atmospheric and oceanic sciences [98–102]. The principal components (PCs) are generalized from straight lines to curves, thus the NLPCA helps to extract PCs either linear or not. This could improve

seasonal rainfall forecast skills because it is well known that most of atmospheric/climate relationships are not linear as always assumed. Each predictor was first screened using R^2 before being fed into the NLPCA. However, due to the high computational time of NLPCA the number of PCs is narrowed in considering only the three best PCs in the process. Figure 4 presents the entire process of the NLPCA seasonal forecast model. More details on the way NLPCA model works and its difference with the ordinary PCA can be found in Scholz *et al.* [97].

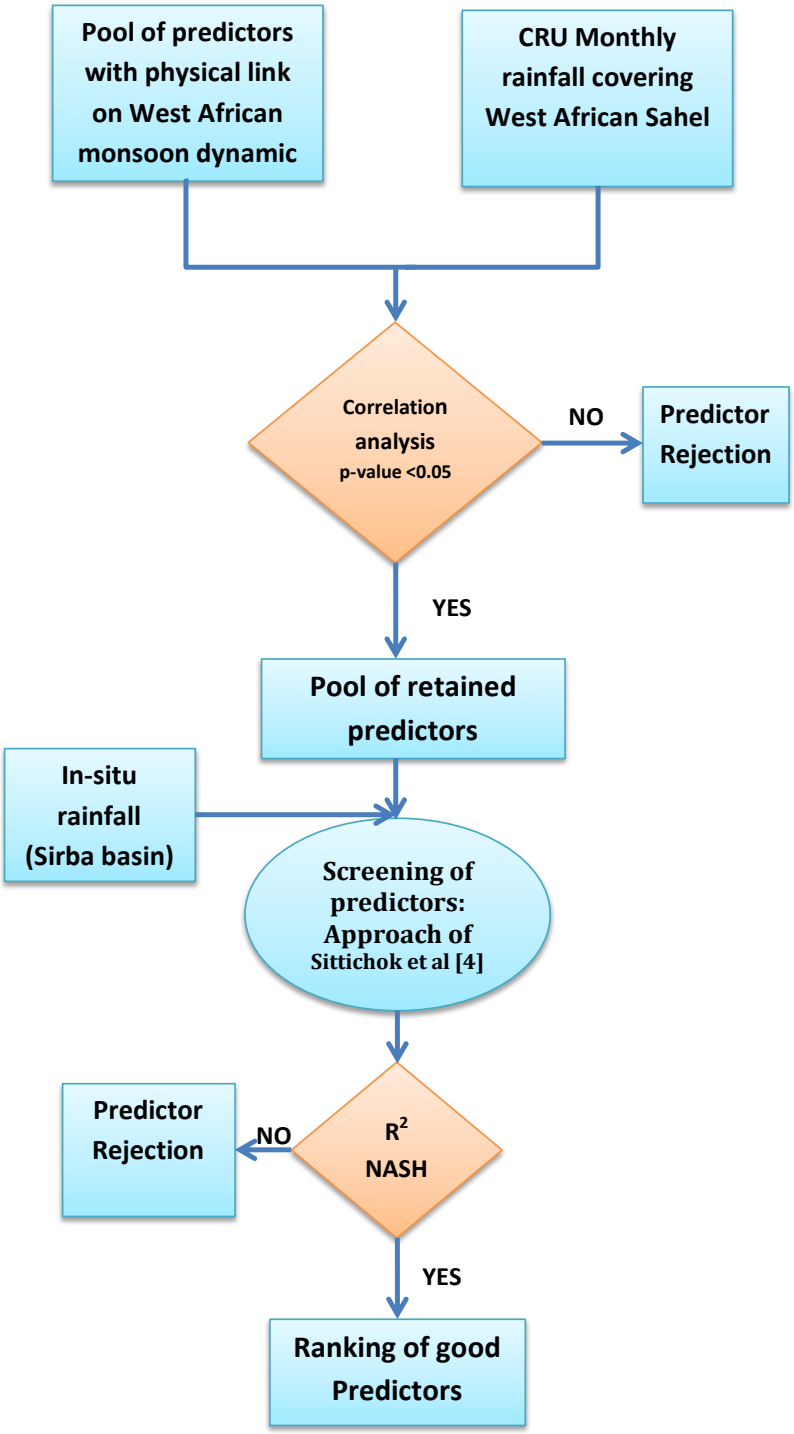

Figure 3. Steps for the selection of predictors.

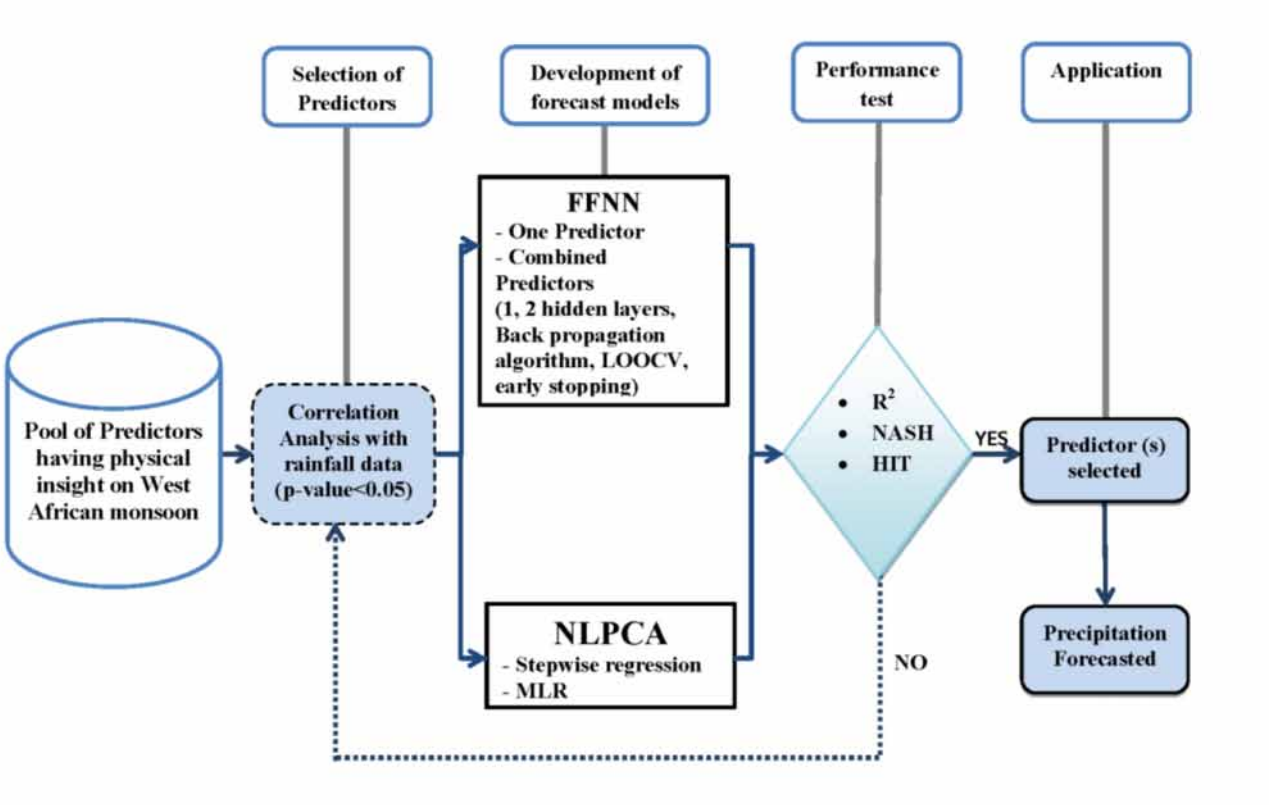

Figure 4. Developed non-linear statistical approach for rainfall forecast.

3.5.2. Feedforward Neural Network

The feedforward neural network (FFNN) is just tested in this work because to show its performance which is somehow poor. For more details on this method, the reader can refer to [103–109].

4. Results and Discussions

4.1. Selected Predictors and Lag Time Period

In the preliminary setting of a pool of predictors, the synchronous correlations between predictors-predictand (*i.e.*, correlations between rainfall and predictors averaged over JAS period) have revealed the presence of the largest correlations for the period 1970–2010. Thus, it was used as the reference study period. For instance, Figure 5 presents the correlation between rainfall and SLP over this time period with a lag time of three months between the two variables.

During the second step dedicated to selecting the predictors, the time window (or season) which yielded the best Nash coefficient (and therefore the optimal lag time) was determined. Tables 3–5 summarize the final selected predictors used to forecast seasonal rainfall using combined linear methods, NLPCA and FFNN, respectively. It is obvious that for all models the best predictors according to the forecast skills are AirTemp, RHUM and SLP. In addition, the lag time (eight months lead time on average) obtained for most predictors is large enough to develop early warning systems for the decision makers and socio-economic actors about the issue of the forthcoming rainy season.

4.2. Seasonal Rainfall Forecast

The performance of the combined linear models showed that AirTemp (from Pacific Tropical North), RHUM (from Mediterranean East) and SLP (from Atlantic tropical South) are the best predictors with respective Nash coefficients of 0.53, 0.52 and 0.46 (see Table 3). They have also the best coefficients of determination (53%, 58%, 48%) and Hit rate scores (67.9%, 64.3%, 60.7%), respectively. While SST (from Atlantic Ocean) obtained 0.34, 43%, and 58.5% as Nash, R^2 and Hit rate scores, respectively. These results from the predictors AirTemp, RHUM, and SLP seem to be better than those obtained in [4] who used linear methods to forecast seasonal rainfall in the same area based on Pacific and Atlantic SSTs as predictor. They obtained 0.45, 0.38 and 66.67% respectively for R^2, Nash, and Hit rate score. Figures 6 and 7 present the observed and simulated seasonal rainfall for combined linear models.

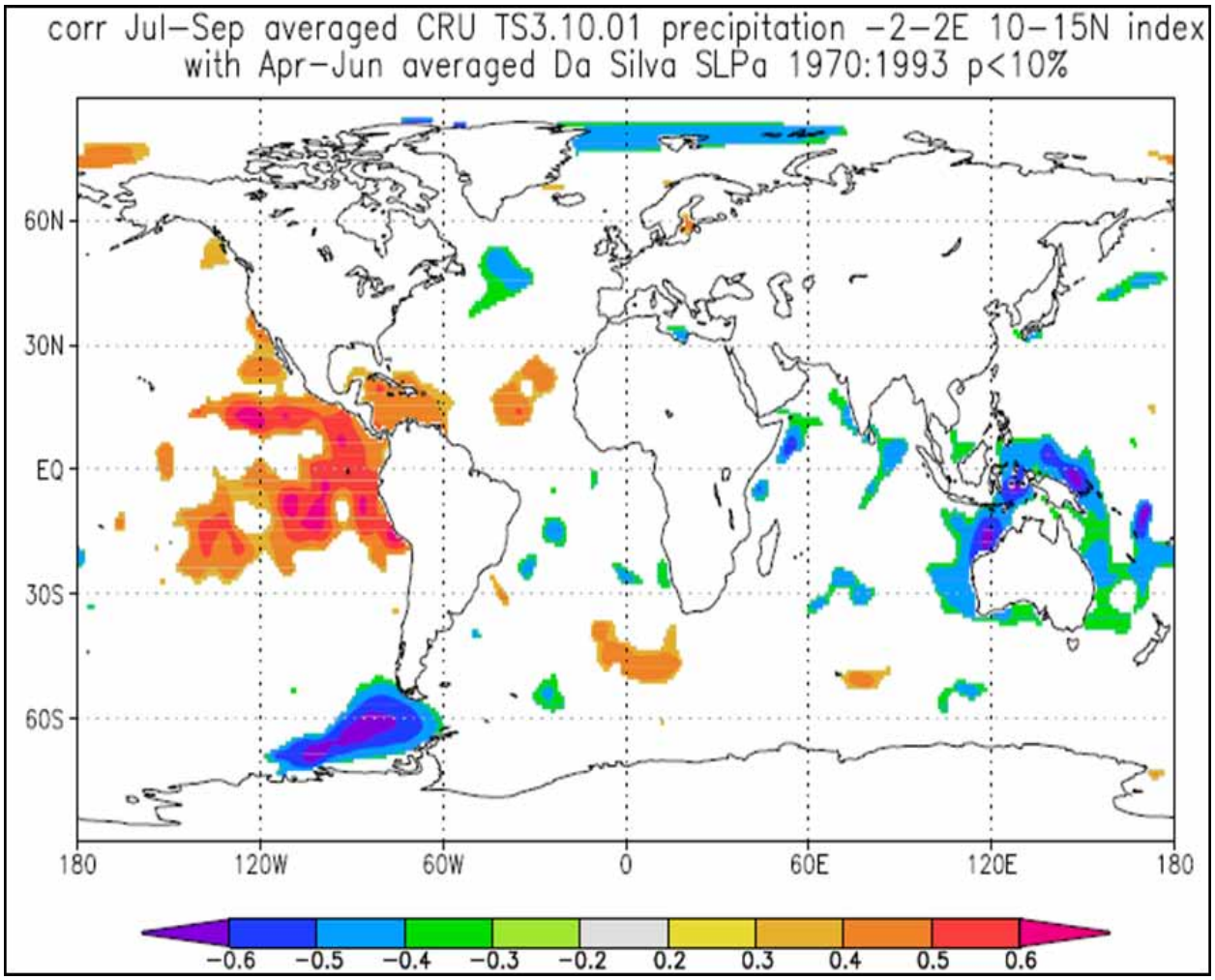

Figure 5. Correlation map between seasonal precipitation and sea level pressure (Da Silva analysis, sea).

Table 3. Combined linear methods for seasonal rainfall forecast.

PREDICTOR	NMAX*	R^2	Nash coef.	HIT Score	Best period M1-M2**	Lag period
Sea Level Pressure (SLP) at 1000hPa	50	0.48	0.46	60.71	17-18	0
Relative Humidity (RHUM) at 1000hPa	80	0.58	0.52	64.29	10-10	8 months
Air Temperature (AirTemp) at 1000hPa	10	0.530	0.527	67.86	1-4	7 months
Meridional Wind (VWND) at 1000hPa	170	0.31	0.28	53.57	5-5	8 months
Zonal Wind (UWND) at 1000hPa	190	0.33	0.324	71.43	11-11	7 months
Sea surface temperature (SST)	30	0.43	0.34	58.54	3-6	12 months

(**) M1=1:12 (January to December); M2=M1:18 (considered month of M1 to the next coming June)

(*) NMAX: number of best grid points retained after screening the predictor grid based on R^2

Table 4. Seasonal rainfall forecast model skills using non-linear principal component analysis (NLPCA).

PREDICTOR	R^2	NASH	HIT score	Lag time Period
Sea Level Pressure (SLP) at 1000hPa	0.32	0.31	53.57	9 months
Relative Humidity (RHUM) at 1000hPa	0.36	0.36	53.57	7 months
Air Temperature (AirTemp) at 1000hPa	0.46	0.45	60.71	8 months

Table 5. Feedforward neural network (FFNN) model (single predictor) output for Sirba seasonal rainfall forecast.

Predictors	R^2	Nash	HIT score (%)	Lag time (months)
AirTemp	0.26	0.20	48.24	4
RHUM	0.18	0.10	29.12	4
SLP	0.21	0.09	18.03	2
SST	0.18	0.044	11.49	5

For the NLPCA model, the issued seasonal forecast skills can be judged satisfactory regarding the short study period considered, because non-linear models need longer study periods to over perform the linear ones. Results showed that the predictor AirTemp (R^2: 0.46; Nash: 0.45; HIT: 60.7%) was the best, and then followed by RHUM and SLP, respectively. It was also found that this method provides a to larger lag time compared to combined non-linear methods despite of its relative low forecast skills. Table 4 presents the model performance and the lag time, while Figure 8 illustrates some of the rainfall forecast obtained from the NLCPA model using, respectively, the predictors AirTemp and RHUM.

Overall, the set of linear models performs better than the non-linear ones. This suggests that there is less benefit using non-linear methods when dealing with small samples, as found in previous studies [27,96,102].

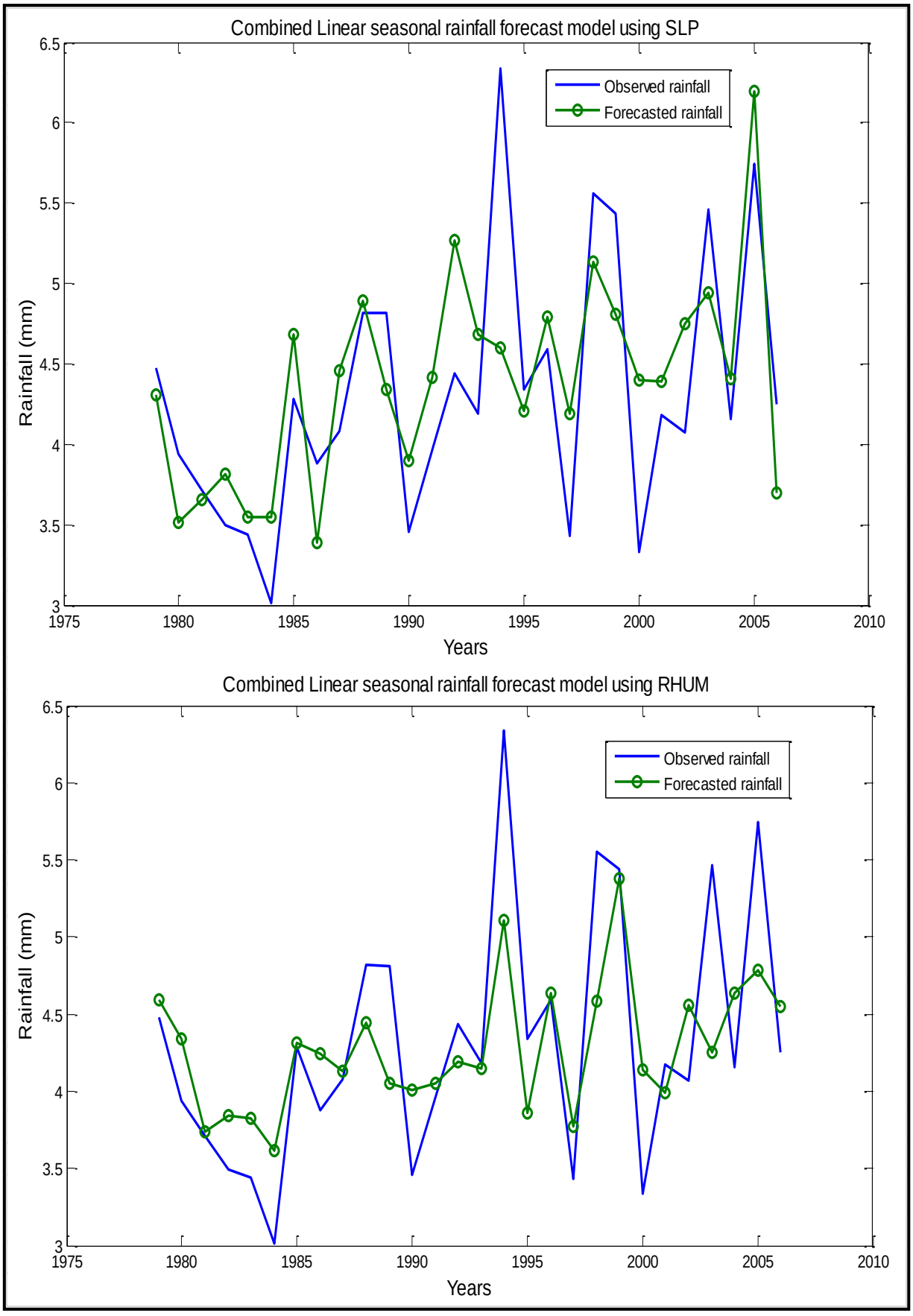

Figure 6. Combined linear model for seasonal rainfall forecast using SLP (upper panel) and RHUM (lower panel).

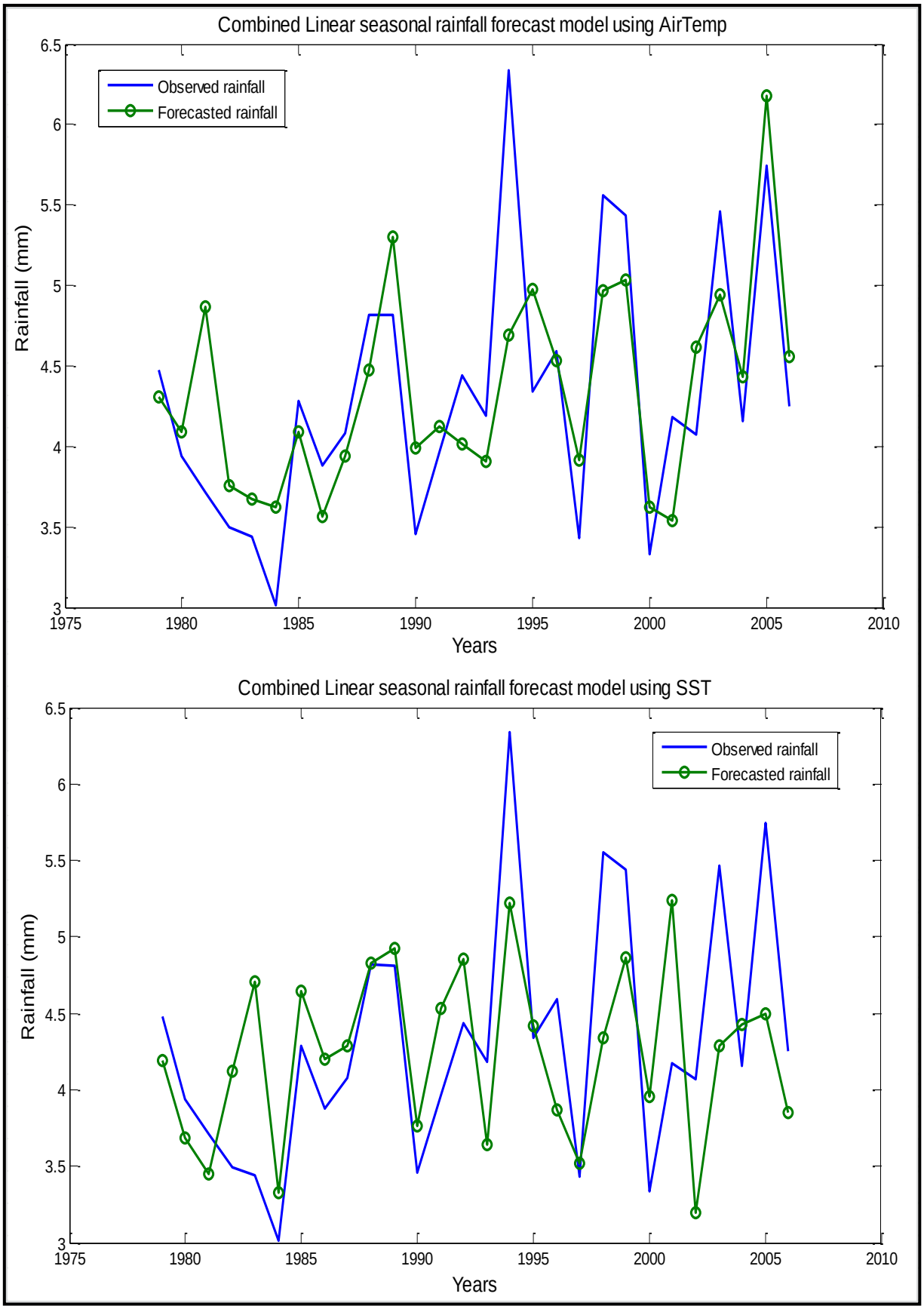

Figure 7. Combined linear model for seasonal rainfall forecast using AirTemp (upper panel) and SST (lower panel).

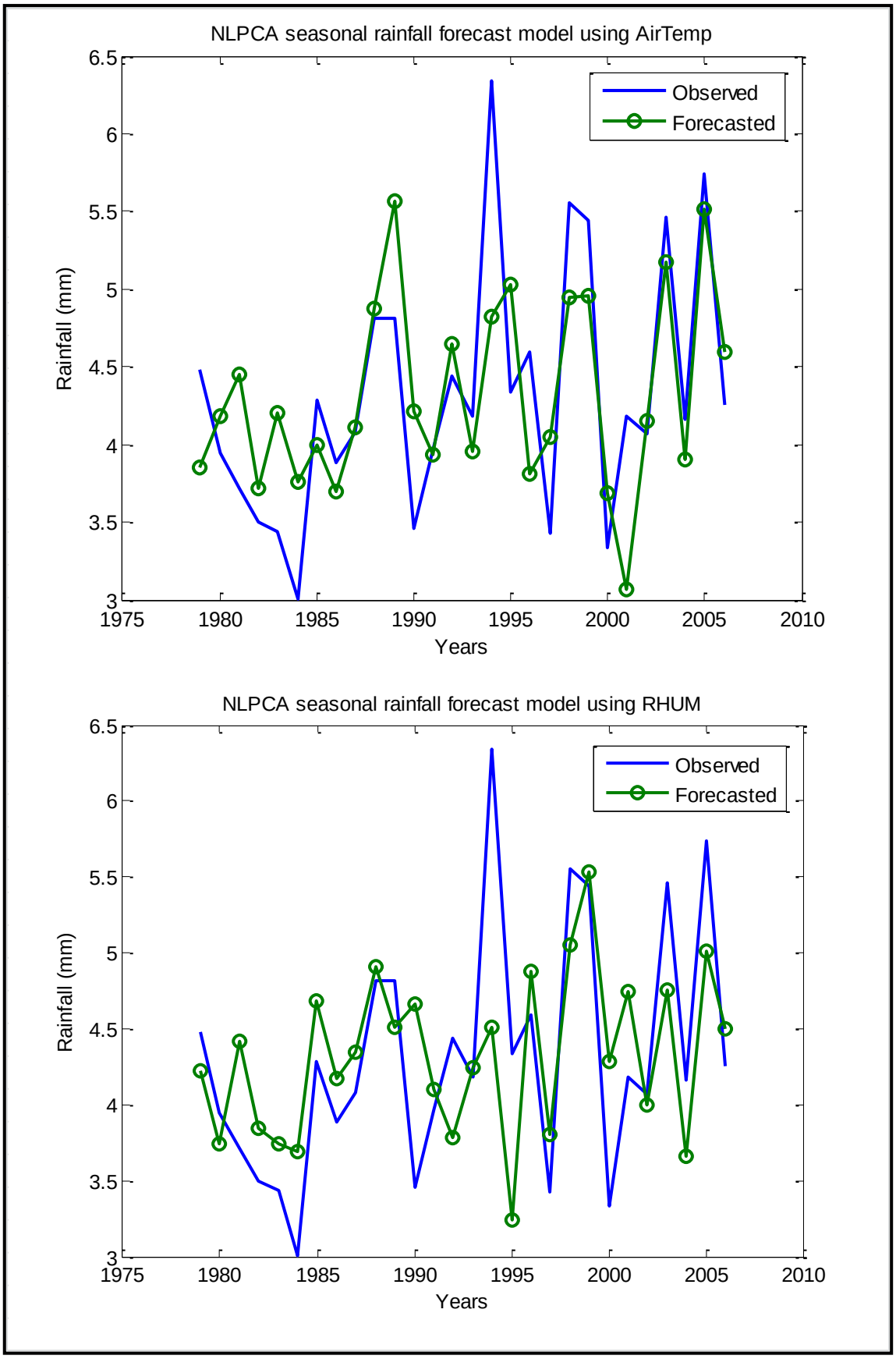

Figure 8. NLPCA seasonal rainfall forecast model using AirTemp (upper panel) and RHUM (lower panel).

5. Conclusions

Two non-linear methods and a combined linear approach were used to forecast JAS (July to September) rainfall on the Sirba watershed, West Africa. Predictors were first screened using a series of steps to isolate those having the highest predictive power. At the end of the process three predictors, air temperature (from Pacific Tropical North), sea level pressure (from Atlantic Tropical South) and relative humidity (from Mediterranean East) were retained and tested as inputs for seasonal rainfall forecasting models. Forecast performances were compared using R^2, Nash and HIT. Results showed that the combined linear approach performed better than the non-linear models. The best forecasts were obtained using air temperature as predictor (R^2 = 53%; Nash = 0.53; HIT = 67.9%; Lead-time = 7 months). The next best model uses relative humidity as predictor (R^2 = 58%; Nash = 0.52; HIT = 64.3%, Lead-time = eight months). Nonlinear Principal Component Analysis (NLPCA) was the best non-linear method while FFNN performed poorly. These new predictors found in this study could lead to better forecasts of seasonal rainfall over West Africa, an issue which has challenged forecasters over many years. This paper also helped understanding that non-linear methods could also be used instead of the usual linear methods. The specificity of this work is the use of other predictors rather than the SST which gave acceptable results than the SST. However, the limit of the approach resides on the small length of data used. Therefore, to generalize the results for other scientists, it is recommended that during the forecast a Sahelian global index must be constructed using CRU data while examining its correlation with the index of the watershed and the skill of models. As a future step of this work, a multi-model approach will be used to compare the resulting skills to that of the best model.

Acknowledgements

The authors would like to thank the International Research Initiative on Adaptation to Climate Change (IRIACC) program through the International Development Research Center (Canada) for funding this research.

Author Contributions

Abdouramane Gado Djibo developed the models, performed analyses and wrote the paper. Nathalie Philippon, Ousmane Seidou, Harouna Karambiri, Hadiza Moussa Saley, Ketvara Sittichok and Jean Emmanuel Paturel contributed to analysis and interpretation of results. Nathalie Philippon, Ousmane Seidou, and Ketvara Sittichok proofread the manuscript and contributed to answer reviewers' comments.

Conflicts of Interest

The authors declare no conflict of interest.

References

1. Gado Djibo, A.; Seidou, O.; Karambiri, H.; Sittichock, K.; Paturel, J.E.; Saley, H.M. Development and assessment of non-linear and non-stationary seasonal rainfall forecast models for the Sirba watershed, West Africa. *J. Hydrol. Reg. Stud.* **2015**, *4*, 134–152.
2. Sarr, M.A.; Gachon, P.; Seidou, O.; Bryant, C.R.; Ndione, J.A.; Comby, J. Inconsistent linear trends in Senegalese rainfall data. *Hydrol. Sci. J.* **2014**, doi:10.1080/02626667.2014.926364.
3. Sarr, M.A.; Zorom é, M.; Seidou, O.; Bryant, C.R.; Gachon, P. Recent trends in selected extreme precipitation indices in Senegal-A changepoint approach. *J. Hydrol.* **2013**, *505*, 326–334.
4. Sittichok, K.; Gado Djibo, A.; Seidou, O.; Saley, H.M.; Karambiri, H.; Paturel, J. Statistical seasonal rainfall and streamflow forecasting for the Sirba watershed, using sea surface temperature. *Hydrol. Sci. J.* **2014**, doi:10.1080/02626667.2014.944526.
5. Samimi, C.; Fink, A.H.; Paeth, H. The 2007 flood in the Sahel: causes, characteristics and its presentation in the media and FEWS NET. *Nat. Hazards Earth Syst. Sci.* **2012**, *12*, 313–325.
6. Brooks, N. *Drought in the African Sahel: Long term perspectives and future prospects*; University of East Anglia: Norwich, UK, 2004.
7. Amadou, A.; Gado Djibo, A.; Seidou, O.; Sittichok, K.; Seidou Sanda, I. Changes to flow regime on the Niger River at Koulikoro under a changing climate. *J. Hydrol. Sci.* **2014**, doi: 10.1080/02626667.2014.916407.
8. Ibrahim, B.; Karambiri, H.; Polcher, J.; Yacouba, H.; Ribsttein, P. Changes in rainfall regime over Burkina Faso under the climate change conditions simulated by 5 regional climate models. *Clim. Dyn.* **2014**, *42*, 1363–1381.
9. Le Barbe, L.; Lebel, T.; Tapsoba, D. Rainfall variability in West Africa during the years 1950–90. *J. Clim.* **2002**, *15*, 187–202.
10. Janicot, S.; Trzaska, S.; Poccard, I. Summer Sahel-ENSO teleconnection and decadal time scale SST variations. *Clim. Dyn.* **2001**, *18*, 303–320.
11. Fontaine, B.; Janicot, S. Sea surface temperature fields associated with West African rainfall anomaly types. *J. Clim.* **1996**, *9*, 2935–2940.
12. Folland, C.K.; Palmer, T.N.; Parker, D.E. Sahel rainfall and worldwide sea temperature 1901–1985. *Nature* **1986**, *320*, 602–607.
13. Hastenrath, S. Decadal scale changes of the circulation in the tropical Atlantic sector associated with Sahel drought. *Int. J. Climatol*. **1990**, *20*, 459–472.
14. Lamb, P.J. West African water variations between recent contrasting Subsaharan droughts. *Tellus* **1983**, *35*, 198–212.
15. Lamb, P.J.; Peppler, R.A. Further case studies of tropical Atlantic surface atmospheric and oceanic patterns associated with sub-Saharan drought. *J. Clim.* **1992**, *5*, 476–488.
16. Nicholson, S.E. Rainfall and atmospheric circulation during drought periods and wetter years in West Africa. *Mon. Wea. Rev*. **1981**, *109*, 2191–2208.
17. Nicholson, S.E. Land surface processes and Sahel climate. *Rev. Geophys*. **2000**, *38*, 117–139.
18. Nicholson, S.E. The West African Sahel: A review of recent studies on the rainfall regime and its interannual variability. *ISRN Meteor*. **2013**, *2013*, 453–521.

19. Kwon, H.H.; Brown, C.; Xu, K.; Lall, U. Seasonal and annual maximum streamflow forecasting using climate information: application to the Three Gorges Dam in the Yangtze River basin, China. *Hydrol. Sci. J.* **2009**, *54*, 582–595.
20. Liu, Z.; Alexander, M. Atmospheric bridge, oceanic tunnel, and global climatic teleconnections. *Rev. Geograph.* **2007**, *45*, 1–34.
21. Gaetani, M.; Fontaine, B. Interaction between the West African Monsoon and the summer Mediterranean climate: An overview. *Fisica de la Tierra* **2013**, *25*, 41–55.
22. Jung, T.; Ferranti, L.; Tompkins A.M. Response to the summer 2003 Mediterranean SST anomalies over Europe and Africa. *J. Cimate*, **2006**, 19, 5439-5454.
23. Camberlin, P.; Janicot, S.; Poccard, I. Seasonality and atmospheric dynamics of the teleconnection between African rainfall and tropical sea-surface temperature: Atlantic VS. ENSO. *Int. J. Clim.* **2001**, *21*, 973–1005.
24. Rowell, D.P. Teleconnections between the tropical Pacific and the Sahel. *Q. J. R. Meteorol. Soc.* **2001**, *127*, 1683–1706.
25. Chase, T.N.; Pielke S.R.; Avissar, R. Teleconnections in the Earth System. Encyclopedia of Hydrological Sciences. Available online: http://onlinelibrary.wiley.com/doi/10.1002/0470848944.hsa190/pdf (accessed on 12 August 2014).
26. Ndiaye, O.; Ward, M.N.; Thiaw, W.M. Predictability of seasonal Sahel rainfall using GCMs and lead-time improvement through the use of a couple model. *J. Clim.* **2011**, *24*, 1931–1949.
27. Bouali, L. Prévisibilité et Prévision Statistico-Dynammique des Saisons des Pluies Associées à la Mousson Ouest Africaine à Partir d'Ensembles Multi-modèLes. Ph.D. Thesis, Université de Bourgogne, Bourgogne, France, 2009.
28. Garbrecht, J.D.; Schneider, J.M.;, Van Liew, M.W. Monthly runoff predictions based on rainfall forecasts in a small Oklahoma Watershed. *J. Am. Water Resour. Assoc.* **2007**, *42*, 1285–1295.
29. Tuteja, N.K.; Shin D.; Laugesen, R.; Khan, U.; Shao, Q.; Wang, E.; Li, M.; Zheng, H.; Kuczera, G.; Kavetski, D.; *et al. Experiment evaluation of the dynamic seasonal streamflow forecasting approach*; Bureau of Meteorology: Melbourne, Vic, Australia, 2011.
30. Chiew, F.H.S.; McMahon, T.A. Global ENSO-streamflow teleconnection, streamflow forecasting and interannual variability. *Hydrol. Sci. J.* **2002**, *47*, 505–522.
31. Ndiaye, O.; Goddard, L.; Ward, M.N. Using regional wind fields to improve general circulation model forecasts of July-September Sahel rainfall. *Int. J. Clim.* **2009**, *29*, 1262–1275.
32. Wang, E.; Zhang, Y.; Luo, J.; Chiew, F.; Wang, Q.J. Monthly and seasonal streamflow forecasts using rainfall-runoff modeling and historical weather data. *Water Resour. Res.* **2011**, *47*, 1–13.
33. Yossef, N.C.; Winsemius, H.; Weerts, A.; Beek, R.V.; Bierkens, F.P. Skill of global seasonal streamflow forecasting system, relative roles of initial conditions and meteorological forcing. *Water Resour. Res.* **2013**, *49*, 4687–4699.
34. Mohino, E.; Rodriguez-Fonseca, B.; Mechoso, C.R.; Gervois, S.; Ruti, P.; Chauvin, F. Impacts of the tropical Pacific/Indian Oceans on the seasonal cycle of the West African monsoon. *J. Clim.* **2011**, *24*, 3878–3891.
35. Rodriguez-Fonseca, B.; Janicot, S.; Mohino, E.; Losada, T.; Bader, J.; Caminade, C.; Chauvin, F.; Fontaine, B.; Garcia-Serrano, J.; Gervois, S.; *et al.* Interannual and decadal SST-forced responses of the West African monsoon. *Atmos. Sci. Lett.* **2011**, *12*, 67–74.

36. Singh, O.P. Cause-effect relationships between sea surface temperature, precipitation and sea level along the Bangladesh coast. *Theor. Appl. Clim.* **2001**, *68*, 233–243.
37. Garcia-Serrano, J.; Doblas-Reyes, F.J.; Haarsma, R.J.; Polo, I. Decadal prediction of the dominant West African monsoon rainfall modes. *J. Geophys. Res. Atmos.* **2013**, *118*, 5260–5279.
38. Philippon, N.; Doblas-Reyes, F.J.; Ruti, P.M. Skill, reproducibility and potential predictability of the West African monsoon in coupled GCMs. *Clim. Dyn.* **2010**, *35*, 53–74.
39. Rodrigues L.R.L.; Garcia-Serrano, J.; Doblas-Reyes, F. Seasonal prediction of the intraseasonal variability of the West African monsoon precipitation. *Fisica de la Tierra* **2013**, *25*, 73–87.
40. Sultan, B.; Janicot, S.; Diedhiou, A. The West African monsoon dynamics. Part I: Documentation of intraseasonal variability. *J. Clim.* **2003**, *16*, 3389–3406.
41. Marteau, R. Cohérence Spatiale et prEvisibilité Potentielle des Descripteurs intrasaisonniers de la Saison des Pluies en Afrique Soudano-Sahélienne : Application à la Culture du mil dans la réGion de Niamey. Ph.D. Thesis, Université de Bourgogne, Bourgogne, France, 2010.
42. Garric, G.; Douville, H.; Déqué, M. Prospects for improved seasonal predictions of monsoon precipitation over Sahel. *Int J. Climatol.* **2002**, *22*, 331–345.
43. Tippet, M.K.; Giannini, A. Potentially predictable components of African summer rainfall in an SST-forced GCM simulation. *J. Clim.* **2006**, *19*, 3133–3144.
44. Batté, L.; Déqué, M. Seasonal predictions of precipitation over Africa using coupled ocean-atmosphere general circulation models: Skill of the ENSEMBLES project multimodel ensemble forecasts. *Tellus A* **2011**, *63*, 283–299.
45. Olivry, J.C. Evolution réCente des réGimes Hydrologiques en Afrique Intertropicale; Presses Universitaires de Nancy: Nancy, France, 1993.
46. Rowell, D.P.; Folland, C.K.; Maskell, K.; Ward, M.N. Variability of summer rainfall over Tropical North Africa (1906–1992): Observations and modelling. *Q. J. R. Meteorol. Soc.* **1995**, *121*, 669–704.
47. Solomon, A.; Goddard, L.; Kumar, A.; Carton, J.; Deser, C.; Fukumori, I.; Greene, A.M.; Hegerl, G.; Kirtman, B.; Kushnir, Y.; *et al.* Distinguishing the roles of natural and anthropogenically forced decadal climate variability. *Bull. Am. Meteorol. Soc.* **2011**, *92*, 141–156.
48. Gaetani, M.; Mohino, E. Decadal prediction of the Sahelian precipitation in CMIP5 simulations. *J. Clim.* **2013**, *26*, 7708–7719.
49. Hastenrath, S. Interannual variability and annual cycle: Mechanisms of circulation and climate in the Tropical Atlantic Sector. *Mon. Weather. Rev.* **1984**, *112*, 1097–1107.
50. Druyan, L.M. The sensitivity of sub-Saharan precipitation to Atlantic SST. *Clim. Chang.* **1991**, *18*, 17–36.
51. Lamb, P.J.; Peppler, R.A. West Africa. In *Teleconnections Linking Worldwide Climate Anomalies*, Glantz, M.H., Katz, R.W., Nicholls, N., Eds.; Cambridge University Press: Cambridge, England, 1991; pp. 121–189.
52. Janicot, S. Spatio-temporal variability of West African rainfall. Part II: associated surface and air mass characteristics. *J. Clim.* **1992**, *5*, 499–511.
53. Janicot, S.; Moron, V.; Fontaine, B. Sahel droughts and ENSO dynamics. *Geophys. Res. Lett.* **1996**, *23*, 515–518.
54. Moron, V. Guinean and Sahelian rainfall anomaly indices at annual and monthly scales (1933–1990). *Int. J. Clim.* **1994**, *14*, 325–341.

55. Janicot, S.; Harzallah, A.; Fontaine, B.; Moron, V. West African monsoon dynamics and Eastern Equatorial Atlantic and Pacific SST anomalies (1970–88). *J. Clim.* **1998**, *11*, 1874–1882.
56. Rowell, D.P. The impact of Mediterranean SSTs on the Sahelian rainfall season. *J. Clim.* **2003**, *16*, 849–862.
57. Gaetani, M.; Fontaine, B.; Roucou, P.; Baldi, M. Influence of the Mediterranean Sea on the West African monsoon: intraseasonal variability in numerical simulations. *J. Geophys. Res.* **2010**, *115*, doi: 10.1029/2010JD014436.
58. Polo, I.; Ullmann, A.; Roucou, P.; Fontaine, B. Weather regimes in the Euro-Atlantic and Mediterranean sector and relationship with West African rainfall over the period 1989–2008 from a self-organizing maps approach. *J. Clim.* **2011**, *24*, 3423–3432.
59. Shaman, J.; Tziperman, E. An atmospheric teleconnection linking ENSO and Southwestern European precipitation. *J. Clim.* **2011**, *24*, 124–139.
60. Lopez-Parages, J.; Rodriguez-Fonseca, B. Multidecadal modulation of El Niño influence on the Euro-Mediterranean rainfall. *Geophys. Res. Lett*. **2012**, *39*, doi: 10.1029/2011GL050049.
61. Webster, P.J.; Magana, V.O.; Palmer, T.N.; Shukla, J.; Tomas, R.A.; Yanai, M.; Yasunari, T. The monsoon: Processes, predictability and prediction. *J. Geophys. Res.* **1998**, *103*, 14451–14510.
62. Eltahir, E.A.B. Role of vegetation in sustaining large-scale atmospheric circulations in the tropics. *J. Geophys. Res.* **1996**, *101*, 4255–4268.
63. Philippon, N.; Fontaine, B. The relationship between the Sahelian and previous 2nd Guinean rainy seasons: A monsoon regulation by soil wetness. *Ann. Geophys.* **2002**, *20*, 575–582.
64. Hall, N.M.J.; Peyrillé, P. Dynamics of the West African Monsoon. *J. Phys. IV France* **2006**, *139*, 81–99.
65. Zheng, X.; Eltahir, E.A.B. The role of vegetation in the dynamics of West African monsoons. *J. Clim.* **1998**, *11*, 2078–2096.
66. Wang, G.; Eltahir, E.A.B. Role of vegetation dynamics in enhancing the low frequency variability of the Sahel rainfall. *Water Resour*. **2000**, *36*, 1013–1021.
67. Zeng, N.; Neelin, J.D.; Lau, K.M.; Tucker, C.J. Enhancement of interdecadal climate variability in the Sahel by vegetation interaction. *Science* **1999**, *286*, 1537–1540.
68. Cook, K.H. Generation of the African easterly jet and its role in determining West African precipitation. *J. Clim.* **1999**, *12*, 1165–1184.
69. Douville, H.; Chauvin, F.; Broqua, H. Influence of soil moisture on the Asian and African monsoons. Part I: Mean monsoon and daily precipitation. *J. Clim.* **2001**, *14*, 2381–2403.
70. Douville, H. Influence of soil moisture on the Asian and African monsoons. Part II: Interannual variability. *J. Clim.* **2002**, *15*, 701–720.
71. Douville, H. Assessing the influence of soil moisture on seasonal climate variability with AGCMs. *J. hydrometeorol.* **2003**, *4*, 1044–1066.
72. Mara, F. Développement et analyse des critères de vulnérabilité des populations sahéliennes face à la variabilité du climat: le cas de la ressource en eau dans la vallée de la Sirba au Burkina Faso. Ph.D. Thesis. Université du Québec à Montréal, Montréal, QC, Canada, 2010.
73. Taweye, A. Contribution à l'étude hydrologique du bassin versant de la Sirba à Garbé-Kourou. Centre Régional AGRHYMET: Ouagadougou, Burkina Faso, 1995.
74. Ball, J.E.; Luk, K.C. Modeling spatial variability of rainfall over a catchment. *J. Hydrol. Eng.* **1998**, *3*, 122–130.

75. British Atmospheric Data Centre (BADC). High-Resolution Gridded Datasets (and Derived Products). Available Online: http://www.cru.uea.ac.uk/cru/data/hrg/ (accessed on 9 September 2015).
76. International Research Institute for Climate and Society (IRI) Data Library. Available Online: http://iridl.ldeo.columbia.edu (accessed on 9 September 2015).
77. Gallée, H.; Moufouma-Okia, W.; Bechtold, P.; Brasseur, O.; Dupays, I.; Marbaix, P.; Messager, C.; Ramel, R.; Lebel, T. A high-resolution simulation of a West African rainy season using a regional climate model. *J. Geophys. Res*. **2004**, *109*, doi: 10.1029/2003JD004020.
78. Thorncroft, C.; Blackburn, M. Maintenance of the African easterly jet. *Q. J. R. Meteorol. Soc*. **1999**, *125*, 763–786.
79. Grist, J.P.; Nicholson, S. A Study of the Dynamic Factors Influencing the Rainfall Variability in the West African Sahel. *J. Clim.* **2001**, *14*, 1337–1359.
80. Janicot, S.; Mounier, F.; Hall, N.M.J.; Leroux, S.; Sultan, B.; Kiladis, G.N. Dynamics of the West African monsoon. Part IV: Analysis of 25-90-Day variability of convection and the role of the Indian monsoon. *J. Clim.* **2009**, *22*,1541–1565.
81. Sultan, B. Etude de la Mise en Place de la Mousson en Afrique de l'Ouest et de la Variabilité Intra Saisonnière de la Convection. Applications à la Sensibilité des Rendements Agricoles. Ph.D. Thesis, Université Denis Diderot, Paris, France, 2002.
82. Nicholson, S.; Grist, J. The seasonal evolution of the atmospheric circulation over West Africa and equatorial Africa. *J. Clim*. **2003**, *16*, 1013–1030.
83. Fontaine, B.; Louvet, S.; Roucou, P. Definition and predictability of an OLR based West African monsoon onset. *Int. J. Climatol*. **2008**, *28*, 1787–1798.
84. Flaounas, E.; Janicot, S.; Bastin, S.; Roca, R.; Mohino, E. The role of the Indian monsoon onset in the West African monsoon onset: observations and AGCM nudged simulations. *Clim. Dyn.* **2012**, *38*, 965–983.
85. Guiavarch, C.; Tréguier, A.M.; Vangriesheim, A. Deep currents in the Gulf of Guinea: Along slope propagation of intraseasonal waves. *Ocean Sci.* **2009**, *5*, 141–153.
86. Coëtlogon, G.; Janicot, S.; Lazar, A. Intraseasonal variability of the ocean—Atmosphere coupling in the Gulf of Guinea during boreal spring and summer. *Q. J. R. Meteorol. Soc*. **2010**, *136*, 426–441.
87. Peyrillé, P.; Lafore, J.P. An idealized Two-Dimensional framework to study the West African monsoon. Part II: Large-scale advection and the diurnal cycle. *J. Atmos. Sci*., **2007**, *64*, 2783–2803.
88. Fontaine, B.; Garcia-Serrano, J.; Roucou, P.; Rodriguez-Fonseca, B.; Losada, T.; Chauvin, F.; Gervois, S.; Sijikumar, S.; Ruti, P.; Janicot, S. Impacts of warm and cold situations in the Mediterranean basins on the West African monsoon: observed connection patterns (1979–2006) and climate simulations. *Clim. Dyn.* **2010**, *35*, 95–114.
89. Gu, G.; Adler, R. Seasonal evolution and variability associated with the West African monsoon system. *J. Clim*., **2004**, 17, 3364–3377.
90. Giannini, A.; Saravanan, R.; Chang, P. Oceanic forcing of Sahel rainfall on interannual to interdecadal time scales. *Science* **2003**, *302*, 1027–1030.
91. Baldi, M.; Dalu, G.; Maracchi, G.; Pasqui, M.; Cesarone, F. Heat waves in the Mediterranean: A local feature or a larger-scale effect? *Int. J. Climatol*. **2006**, *26*, 1477–1487.

92. Kalnay, E.; Kanamitsu, M.; Kistler, R.; Collins, W.; Deaven, D.; Gandin, L.; Iredell, M.; Saha, S.; White, G.; Woollen, J.; *et al*. The NCEP/NCAR 40-year reanalysis project. *Bull. Am. Met. Soc.* **1996**, *77*, 437–471.
93. Kistler, R.; Kalnay, E.; Collins, W.; Saha, S.; White, G.; Woollen, J.; Chelliah, M.; Ebisuzaki, W.; Kanamitsu, M.; Kousky, V.; *et al*. The NCEP-NCAR 50-year reanalysis: Monthly means CD-ROM and documentation. *Bull. Am. Met. Soc.* **2001**, *82*, 247–268.
94. Maheras, P.; Kutiel, H. Spatial and temporal variations in the temperature regime in the Mediterranean and their relationship with circulation during the last century. *Int. J. Climatol*. **1999**, *19*, 745–764.
95. Lafore, J.; Flamant, C.; Giraud, V.; Guichard, F.; Knippertz, P.; Mahfouf, J.; Mascart, P.; Williams, E. Introduction to the AMMA special issue on "Advances in understanding atmospheric processes over West Africa through the AMMA field campaign". *Q. J. R. Meteorol. Soc.* **2010**, *136*, 2–7.
96. Broman, D.; Rajagopalan, B.; Hopson, T. Spatiotemporal variability and predictability of Relative Humidity over West African Monsoon Region. *J. Clim.* **2014**, *27*, 5346–5363.
97. Scholz, M.; Martin, F.; Joachim, S. Nonlinear principal component analysis: neural network models and applications. In *principal manifolds for Data visualization and dimension reduction*; Gorban, A.N., Kegl, B., Wunsch, D.C., Zinovyev, A., Eds; Springer: Berlin, Germany, 2007; pp. 44–67.
98. Wu, A.; Hsieh, W.W. The nonlinear Northern Hemisphere atmospheric response to ENSO. *Geophys. Res. Lett*. **2004**, *31*, doi: 10.1029/2003GL018885.
99. Hsieh, W.W. Nonlinear multivariate and time series analysis by neural network methods. *Rev. Geophys.* **2004**, *42*, doi: 10.1029/2002RG000112.
100. Monahan, A.H.; Fyfe, J.C.; Pandolfo, L. The vertical structure of winter time climate regimes of the northern hemisphere extratropical atmosphere. *J. Clim.* **2003**, *16*, 2005–2021.
101. Diamantaras, K.; Kung, S. *Principal Component Neural Networks*. Wiley: Hoboken, NJ, USA, 1996.
102. Jolliffe, I.T.; Stephenson, D.B. *Forecast Verification: A Practitioner's Guide in Atmospheric Science*, 2nd ed.; John Wiley & Sons: Hoboken, NJ, USA, 2012.
103. Tangang, F.T.; Hsieh, W.W.; Tang, B. Forecasting regional sea surface temperatures in the tropical Pacific by neural network models, with wind stress and sea level pressure as predictors. *J. Geogr. Res.* **1998**, *103*, 7511–7522.
104. Canon, A.J.; Mckendry, I. Forecasting all-India summer monsoon rainfall using regional circulation principal components: A comparison between neural network and multiple regression models. *Int. J. Clim.* **1999**, *19*, 1561–1578.
105. Badr, H.S.; Zaitchik, B.F.; Guikema, S.D. Application of statistical models to the prediction of seasonal rainfall anomalies over the Sahel. *J. Appl. Meteor. Climatol*. **2014**, *53*, 614–636.
106. El-Shafie, A.H.; El-Shafie, A.; El-Magzoghi, H.G.; Shehata, A.; Taha, M.R. Artificial neural network technique for rainfall forecasting applied to Alexandria, Egypt. *Int. J. Phys. Sci.* **2011**, *6*, 1306–1316.
107. Ansari, H. Forecasting Seasonal and Annual Rainfall Based on Nonlinear Modeling with Gamma Test in North of Iran. *Int. J. Eng. Pract. Res.* **2013**, *2*, 16–29.
108. Hung, N.Q.; Babel, M.S.; Weesakul, S.; Tripathi, N.K. An artificial neural network for rainfall forecasting in Bangkok, Thailand. *Hydrol. Earth Sys. Sci. Discuss.* **2008**, *5*, 183–218.

109. Philippon, N. Une Nouvelle Approche Pour la Prévision Statistique des Précipitations Saisonnières en Afrique de l'Ouest et de l'Est: Méthodes, Diagnostics (1968–1998) et Applications (2000–2001). Ph.D. Thesis, Université de Bourgogne, Dijon, France, 2002.